Astrodynamics Vol. 7, No. 2, 229–249, 2023 https://doi.org/10.1007/s42064-022-0154-0

Natural coupled orbit–attitude periodic motions in the perturbed-CRTBP including radiated primary and oblate secondary

Majid Bakhtiari[1](✉), **Ehsan Abbasali**[2], **Siavash Sabzy**[1], **and Amirreza Kosari**[2]

1. School of Advanced Technologies, Iran University of Science and Technology, Narmak, Tehran 16844, Iran
2. Aerospace Group, Faculty of New Sciences and Technologies, University of Tehran, North Kargar Street, Tehran, Iran

ABSTRACT

This study investigated periodic coupled orbit–attitude motions within the perturbed circular restricted three-body problem (P-CRTBP) concerning the perturbations of a radiated massive primary and an oblate secondary. The radiated massive primary was the Sun, and each planet in the solar system could be considered an oblate secondary. Because the problem has no closed-form solution, numerical methods were employed. Nevertheless, the general response of the problem could be non-periodic or periodic, which is significantly depended on the initial conditions of the orbit–attitude states. Therefore, the simultaneous orbit and attitude initial states correction (SOAISC) algorithm was introduced to achieve precise initial conditions. On the other side, the conventional initial guess vector was essential as the input of the correction algorithm and increased the probability of reaching more precise initial conditions. Thus, a new practical approach was developed in the form of an orbital correction algorithm to obtain the initial conditions for the periodic orbit of the P-CRTBP. This new proposed algorithm may be distinguished from previously presented orbital correction algorithms by its ability to propagate the P-CRTBP family orbits around the Lagrangian points using only one of the periodic orbits of the unperturbed CRTBP (U-CRTBP). In addition, the Poincaré map and Floquet theory search methods were used to recognize the various initial guesses for attitude parameters. Each of these search methods was able to identify different initial guesses for attitude states. Moreover, as a new innovation, these search methods were applied as a powerful tool to select the appropriate inertia ratio for a satellite to deliver periodic responses from the coupled model. Adding the mentioned perturbations to the U-CRTBP could lead to the more accurate modeling of the examination environment and a better understanding of a spacecraft's natural motion. A comparison between the orbit–attitude natural motions in the unperturbed and perturbed models was also conducted to show this claim.

KEYWORDS

oblate and radiated primary
perturbed periodic orbit–attitude behavior
periodic orbit three-body problem
Lagrangian points

Research Article

Received: 6 June 2022
Accepted: 23 September 2022

1 Introduction

Several instances have shown that controlling the attitude motion of a spacecraft is an essential part of space mission design [1–6]. The angular momentum that acts on the spacecraft body is the major cause of perturbations, while the coupling of the orbital and attitude behaviors of a space vehicle enhances the problem's complexity. Employing an accurate approximation of the orbital motion can improve the precision of an attitude dynamic model. The simple unperturbed circular restricted three-body problem (U-CRTBP) is a classical model that defines the motion of a spacecraft immersed in the gravitational fields of two massive bodies [7–10]. In the restricted three-body problem, or U-CRTBP, there are

✉ bakhtiari_m@iust.ac.ir

five equilibrium points called Lagrangian points, in which the gravitational forces from two massive bodies acting on a third body located at one of these points cancel out each other [7, 11, 12]. Thus, an object can remain at one of these points or move around it with the minimum fuel consumption. There are many types of mission planning research related to the U-CRTBP, which considers a spacecraft as a point mass [13, 14]. Considering the spacecraft as a point mass or ignoring its dimensions and their effect on the orbital motion is reasonable for a small spacecraft (with dimensions of less than 100 m) [4]. On the other hand, a space vehicle's attitude is affected by its orbital motion, even for a spacecraft with small dimensions [15]. Investigating the attitude behavior of a spacecraft using a coupled orbital and attitude motion model is an exciting subject for space communities. The first research in this area was reported in Ref. [16], which analyzed the attitude of an axisymmetric satellite that was considered fixed at a Lagrangian point. Other researchers [11] studied the stability of the pitch motion of spacecraft with different configurations at these points. Some investigations employed quaternion parameters to explains the spacecraft attitude at a Lagrangian point [17, 18]. The researchers in Ref. [4] considered relatively small Lyapunov and halo orbits in the solar system to analyze the attitude responses of a space vehicle using a linear form for the reference path.

Further research explored the rotational stability of an orbit–attitude model of a space vehicle with diverse types of orbits in the U-CRTBP [4, 19, 20]. There are many requirements for a space vehicle revolving along periodic orbits around Lagrangian points in the three-body problem. The major one is the use of the minimum effort for its orbital and attitude control. In addition, periodic patterns could be applied for continuous data transfer. There have been many investigations on periodic orbits in the U-CRTBP [15, 21–24]. For example, periodic orbits about Lagrangian pointsin the U-CRTBP were studied by Qian *et al.* [25]. Ceccaroni *et al.* [26] explained the generation of the halo family in the U-CRTBP. Pontani and Miele [27] investigated periodic image trajectories in Earth–Moon space. Giancotti *et al.* [28] also studied Earth–Moon transfers involving periodic orbits and invariant manifolds. Singh and Cyril-Okeme [29] examined periodic solutions around the collinear equilibrium points in the perturbed restricted three-body problem. Obviously, attitude and orbital motions in such a regime significantly depend on the initial conditions. Consequently, finding appropriate and precise initial conditions in which the whole dynamics of a spacecraft repeat after a period is valuable for space mission design. In addition, these periodic solutions can be used to analyze the problem's dynamics. Significant efforts were made in Ref. [30] to study the coupled orbit–attitude equations of motions numerically. Three-dimensional completely coupled model equations of motions were expressed in Ref. [31]. Other studies [15, 32] found conditions where the space vehicle's rotational and orientational motions remained bounded along periodic orbits. To indicate the natural motions of a space vehicle more accurately, more precise models could be employed.

The orbital motion behavior was examined in the perturbed circular restricted three-body problem (P-CRTBP) in previous studies [33]. Singh and Cyril-Okeme [29] assumed the oblateness of the massive primary in the U-CRTBP. Srivastava *et al.* [33] assumed the Earth's oblateness and the massive primary's radiation pressure when considering the problem. The researchers in Ref. [34] explained the nonlinear stability about libration points within the U-CRTBP framework considering the Earth's oblateness. This research was continued by assuming an oblate secondary and different configurations for a single rigid spacecraft [21].

The present study primarily constructed and analyzed the families of periodic orbital motions in the P-CRTBP. Appropriate initial guesses for the orbital parameters are needed for the initial conditions of periodic orbits in the P-CRTBP. The initial conditions for the family of periodic orbits in the P-CRTBP were found using the proposed periodic orbits correction (POC) algorithm. Then, initial guesses for the periodic attitude motion along derived periodic orbits were obtained using the verified Floquet theory and Poincaré mapping search methods. Each of these search methods was able to recognize different sets of initial guesses for attitudestates. Afterward, these initial guesses for the periodic orbit–attitude motions were refined to gain a precise periodic solution using a correction algorithm. Taking these perturbations into account could assist in comprehending the natural behavior of a space vehicle in these problems.

2 P-CRTBP frame representation

Consider three masses that interact gravitationally. The two more massive bodies, m_1 and m_2, are defined as the

primary attractors (planets of the solar system) and are also simply referred to as primaries; the third body (m) may represent a particle of interest, such as a spacecraft or natural object within the same celestial system. In this study, it was assumed that the Sun was the biggest primary, which was represented by m_1, and the smallest primary (the Earth) was an oblate body, m_2, which was also called the secondary. The primaries moved under the action of their mutual gravitation and circled around each other in a circular orbit. It was supposed that the satellite was vanishingly small compared to the primary masses and had no influence on their motion. After making these assumptions, this study investigated the simultaneous orbit and attitude motions of spacecraft m, which was the object of interest. Thus, three coordinate frames were used in this study. The first was a rotating frame that was introduced by unit vector $\boldsymbol{r}(\hat{x}, \hat{y}, \hat{z})$. Unit vector $\hat{z}$ was orthogonal to the plane of the planets. The second one was the inertial reference described by $\boldsymbol{i}(\hat{X}, \hat{Y}, \hat{Z})$. The initial reference was aligned to the rotating coordinate at the initial time. Both of the introduced frames originated in the gravity center of the primaries. The rotating frame rotated at the constant mean motion, Ω, of the primaries relative to an inertial reference. The primaries always remained on the $\hat{x}$-axis, and the third components of both frames were always aligned. Finally, body frame $\boldsymbol{b}(\hat{b}_1, \hat{b}_2, \hat{b}_3)$ was used to express the orientation and rotation of the spacecraft, as seen in Fig. 1. The ${}^{P}\square^{S}$ notation was used in the current research to render the motion from the S frame that is observed from a P frame. In Fig. 1, ψ is the angle between the vector from the spacecraft's center at distance r and the oblate primary's polar axis.

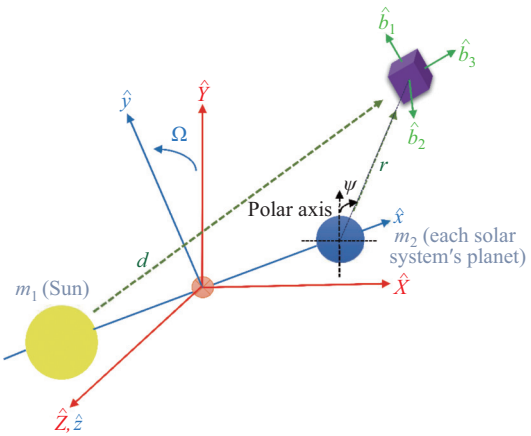

Fig. 1 Required coordinate frames for orbit–attitude of P-CRTBP.

To drive the governing equation of the P-CRTBP, all the units were considered in a non-dimensional form (ndim), such that the total mass of the system, distance between primaries, universal gravitational constant (G), and angular velocity (Ω) were equal to one. The normalized period of the primaries was set equal to 2π. In addition, $\mu = \frac{m_2}{m_1+m_2}$ was introduced as the mass parameter of the system.

3 Orbital equation of motion for P-CRTBP

In this paper, the equations of motion for the P-CRTBP will be derived by applying the Lagrangian function.

$$L = K - V \tag{1}$$

Here, V and K represent the potential field and kinetic energy of the system, respectively, which are derived in Appendix A. After finding the potential field and kinetic equations for a spacecraft in the P-CRTBP, the Euler–Lagrange equation can be applied to extract the orbital equations of motion.

$$f_x(\boldsymbol{x}_{\text{orb}}) = \begin{bmatrix} \ddot{x} = n^2x + 2nv_y - \frac{q(1-\mu)(x+\mu)}{d^3} - \frac{\mu(x+\mu-1)}{r^3} - \frac{3\mu A_2(x+\mu-1)}{2r^3} \\ \ddot{y} = n^2y - 2nv_x - \frac{q(1-\mu)y}{d^3} - \frac{\mu y}{r^3} - \frac{3\mu A_2 y}{2r^3} \\ \ddot{z} = \frac{q(1-\mu)z}{d^3} - \frac{\mu z}{r^3} - \frac{3\mu A_2 z}{2r^3} \end{bmatrix} \tag{2}$$

The equations of motion for the P-CRTBP orbit $f_x(\boldsymbol{x}_{\text{orb}})$, including orbital state vector $\boldsymbol{x}_{\text{orb}} = [x, y, z, v_x, v_y, v_z]$, express the mass center position and velocity of the spacecraft relative to the rotating frame. Equation (2) represents the orbital motion of the P-CRTBP. Because there is no approach to present a closed-form solution, the numerical method must be established. Therefore, the periodic response of the problem is significantly dependent on accurate initial conditions. Identifying periodic orbits for the P-CRTBP is one of the most important goals in the current research. The periodic orbits of the P-CRTBP require appropriate and accurate initial conditions. Howell [35] presented an algorithm that could modify the appropriate and accurate initial conditions of the halo orbits in the U-CRTBP. This article presents a new algorithm to modify the initial conditions of periodic orbits. An essential feature of this proposed algorithm that distinguishes it from the methods presented in previous studies is the algorithm's

ability to expand an initial guess or a known orbit either in the U-CRTBP or P-CRTBP into an infinite number of periodic orbital motions around a collinear Lagrangian point in the P-CRTBP.

4 P-CRTBP periodic orbits correction (POC) algorithm

The algorithm used to extract a family of periodic orbits in the P-CRTBP can be defined in following steps. First, a known orbit in the U-CRTBP [36] around a specific Lagrangian point is considered as a reference. Then, this orbit is corrected using the algorithm proposed for P-CRTBP orbits. In this step, the reference orbit and its period (T) are the inputs of the algorithm, and the output is an orbit with the same period and corrected initial conditions for the P-CRTBP. Based on the algorithm obtained by Ref. [35], two consecutive and perpendicular passages in the (x, z) plane are targeted for the correction algorithm. When the true anomaly of the system is $t_0 = 0$, the initial vector of orbital states is on the (x, z) plane, and the second crossing will be at $t_\mathrm{f} = \frac{T}{2}$. The process of the correction algorithm for orbits in the P-CRTBP incorporates the progression between the last and starting states of the orbital elements. Applying the Newton–Raphson method, the beginning states are iteratively refined until the necessities at the final point are satisfied within an acceptable tolerance. The process can be formulated as Eq. (3):

$$\varsigma_{k+1}^{\mathrm{orbit}} = \varsigma_k^{\mathrm{orbit}} + \boldsymbol{\zeta}\left(\varsigma_k^{\mathrm{orbit}}\right)^{-1} \boldsymbol{\tau}\left(\varsigma_k^{\mathrm{orbit}}\right) \tag{3}$$

where ς_k is the vector of free variables at the kth iteration.

$$\varsigma_k = \left[x_k(t_0), z_k(t_0), v_{k_y}(t_0)\right] \tag{4}$$

$x(t_0)$ indicates the value of the initial x, and $x(t_\mathrm{f})$ is the value of x at the end of the period. $\boldsymbol{\tau}\left(\varsigma_k^{\mathrm{orbit}}\right)$ is the constrain function, which defines the requirements of the algorithm, and at the final point, the relation in Eq. (5) must hold by an acceptable tolerance:

$$\boldsymbol{\tau}(\varsigma_k^{\mathrm{orbit}}) = [y_k(t_\mathrm{f}), v_{k_x}(t_\mathrm{f}), v_{k_z}(t_\mathrm{f})] = 0 \tag{5}$$

$\boldsymbol{\zeta}(\varsigma_k^{\mathrm{orbit}})^{-1}$ contains derivatives of the constrained function variables ($[y_k(t_\mathrm{f}), v_{k_x}(t_\mathrm{f}), v_{k_z}(t_\mathrm{f})]$) with respect to the free variables. Elements of this matrix are corresponding elements of the monodromy matrix at t_f with respect to t_0.

$$\boldsymbol{\zeta}(\varsigma^{\mathrm{orbit}}) = \begin{bmatrix} \overline{\boldsymbol{\Phi}}_{\mathrm{ORB}_{yx}} & \overline{\boldsymbol{\Phi}}_{\mathrm{ORB}_{\mathrm{yz}}} & \overline{\boldsymbol{\Phi}}_{\mathrm{ORB}_{yv_y}} \\ \overline{\boldsymbol{\Phi}}_{\mathrm{ORB}_{v_x x}} & \overline{\boldsymbol{\Phi}}_{\mathrm{ORB}_{v_x z}} & \overline{\boldsymbol{\Phi}}_{\mathrm{ORB}_{v_x v_y}} \\ \overline{\boldsymbol{\Phi}}_{\mathrm{ORB}_{v_z x}} & \overline{\boldsymbol{\Phi}}_{\mathrm{ORB}_{v_z z}} & \overline{\boldsymbol{\Phi}}_{\mathrm{ORB}_{v_z v_y}} \end{bmatrix}$$

Here, $\overline{\boldsymbol{\Phi}}_{\mathrm{ORB}_{yx}}$ is an element of the state transition matrix. For this particular problem, Eq. (7) could designate the state transition matrix (STM) of Eq. (2), where $\boldsymbol{J}_{\mathrm{ORB}}$ is the Jacobian matrix of Eq. (2), and $\boldsymbol{I}$ renders the identity matrix:

$$\begin{cases} \dot{\boldsymbol{\Phi}}_{\mathrm{ORB}}(t,0) = \boldsymbol{J}_{\mathrm{ORB}}(t)\boldsymbol{\Phi}_{\mathrm{ORB}} \\ \boldsymbol{\Phi}_{\mathrm{ORB}}(0,0) = \boldsymbol{I}_{6\times 6} \end{cases} \tag{6}$$

where

$$\boldsymbol{J}_{\mathrm{ORB}}(t) = \left[\frac{\partial \boldsymbol{x}_{\mathrm{orb}}}{\partial \boldsymbol{x}_{\mathrm{orb}}}\right]_{6\times 6} \tag{7}$$

Thus, a periodic orbit in the P-CRTBP has been constructed, which can be extended to a family of orbits by reconsidering this orbit using the algorithm for different periods. For example, $\varsigma_{k+1}^{\mathrm{orbit}}$, which contains the initial condition for an orbit with period T, is the initial guess for an orbit with period $T+\delta$ or $T-\delta$. This means that a known orbit around the Lagrangian point within the P-CRTBP framework can be extended to a family of orbits. The proper value for δ that is used in this research is 0.04 (ndim). In the correction process, it seems that a larger value may cause the divergence of the algorithm for larger periodic orbits about L_1 and L_2. On the other hand, with smaller values for δ, periodic orbits that are very close to each other can be calculated.

5 P-CRTBP coupled orbit–attitude

The most important goal in this study was investigating simultaneous orbital and attitude periodic responses of a space vehicle in the P-CRTBP. The transitional and rotational dynamics for a rigid spacecraft are collected in the form in Eq. (8):

$$\begin{cases} \dot{\boldsymbol{x}}_{\mathrm{orb}} = f_x(\boldsymbol{x}_{\mathrm{orb}}, {}^{\mathrm{i}}\boldsymbol{q}^{\mathrm{b}}, {}^{\mathrm{i}}\boldsymbol{\omega}^{\mathrm{b}}) \\ {}^{\mathrm{i}}\dot{\boldsymbol{q}}^{\mathrm{b}} = f_q({}^{\mathrm{i}}\boldsymbol{q}^{\mathrm{b}}, {}^{\mathrm{i}}\boldsymbol{\omega}^{\mathrm{b}}) \\ {}^{\mathrm{i}}\dot{\boldsymbol{\omega}}^{\mathrm{b}} = f_\omega(\boldsymbol{x}_{\mathrm{orb}}, {}^{\mathrm{i}}\boldsymbol{q}^{\mathrm{b}}, {}^{\mathrm{i}}\boldsymbol{\omega}^{\mathrm{b}}) \end{cases} \tag{8}$$

In Eq. (8), quaternion vector ${}^{\mathrm{i}}\boldsymbol{q}^{\mathrm{b}} = [q_1, q_2, q_3, q_4]$ may explain the spacecraft orientation. In addition, the spacecraft angular velocity with respect to the initial frame rendered in body frame ${}^{\mathrm{i}}\boldsymbol{\omega}^{\mathrm{b}} = [\omega_1, \omega_2, \omega_3]$ could explain the time rate of change for the space vehicle attitude. As is clear in Eq. (8), a variation in the orbital state variables induces a variation in the attitude state variables and vice versa. The set of equations with this property is known as a fully coupled orbit–attitude system. Considering some assumptions will lead to a kind of simplification that will turn this system of equations

into a simplified coupled model (SCM), which means that the time evolution of the orbital state variables is no longer a function of the attitude state variables [30]. The considered assumptions are to regard the spacecraft as a point mass and ignore the spacecraft's dimensions and their effect on its orbital motion (with dimensions smaller than 100 m) [4]. On the other hand, a space vehicle's attitude is affected by its orbital motion, even for a spacecraft with small dimensions [15].

$$\begin{cases} \dot{\boldsymbol{x}}_{\mathrm{orb}} = f_x(\boldsymbol{x}_{\mathrm{orb}}) \\ {}^{\mathrm{i}}\dot{\boldsymbol{q}}^{\mathrm{b}} = f_q({}^{\mathrm{i}}\boldsymbol{q}^{\mathrm{b}}, {}^{\mathrm{i}}\boldsymbol{\omega}^{\mathrm{b}}) \\ {}^{\mathrm{i}}\dot{\boldsymbol{\omega}}^{\mathrm{b}} = f_\omega(\boldsymbol{x}_{\mathrm{orb}}, {}^{\mathrm{i}}\boldsymbol{q}^{\mathrm{b}}, {}^{\mathrm{i}}\boldsymbol{\omega}^{\mathrm{b}}) \end{cases} \tag{9}$$

Considering the SCM, space perturbations influence the attitude dynamics equations of motion by affecting the orbital motion equations. In fact, in this type of coupling, it is sufficient to first consider the effect of perturbations on the orbital equations of motion and then adjust the dynamic equations with these equations. Guzzetti [37] derived these equations for the first time to describe the attitude dynamics of a satellite in the U-CRTBP. Abbasali *et al.* [38] converted these equations into orbital equations of motion in the CRTBP by considering the oblateness of both primaries. Sabzy *et al.* [39] adjusted these equations for use with the elliptic restricted three-body problem (ERTBP). The time propagation of the quaternion equations and angular velocity's time rate equations that regulate the P-CRTBP orbital equation of motions (Eq. (2)) are captured in Fig. 2. Appendix B discusses the parameters used in these equations.

Because there is no approach to present a closed-form solution, the numerical method must be established. To meet the periodic responses of the SCM, appropriate and accurate initial conditions for the orbit–attitude states must be applied. In this article, an orbit–attitude correction is proposed to identify these initial conditions. In addition, because the periodic responses are limited, the proposed algorithm requires an appropriate initial guess as an input. The initial guess for the orbital states can be carefully chosen close to the periodic orbit's initial conditions from the POC algorithm. Appropriate initial guesses for the attitude states were made using the Poincaré mapping and Floquet theory methods.

6 P-CRTBP simultaneous orbit and attitude initial states correction (SOAISC) algorithm

The numerical solution of the SCM system of equations, which depends on the initial conditions, can include different answers such as periodic responses. Thus, the initial conditions play a vital role in achieving the desired solutions. Applying the SOAISC algorithm with an appropriate initial guess as an input can lead to the convergence of the solution to the desired answers. In fact, this algorithm has the task of modifying the initial guess for the vector to achieve eligible initial states (initial conditions). The main idea to develop this algorithm is to use the P-CRTBP coupled orbit–attitude state transition matrix, $\boldsymbol{\Phi}_{\mathrm{OA}}$. This matrix has the ability to connect the system state vector from initial time t_0 to final time t_{f}. If the system state parameter vector for the initial time matches the state vector at final time t_{f}, then the problem has converged to periodic responses, and final time t_{f} will be known as period time T. Thus, it is important to first obtain state transition matrix $\boldsymbol{\Phi}_{\mathrm{OA}}$.

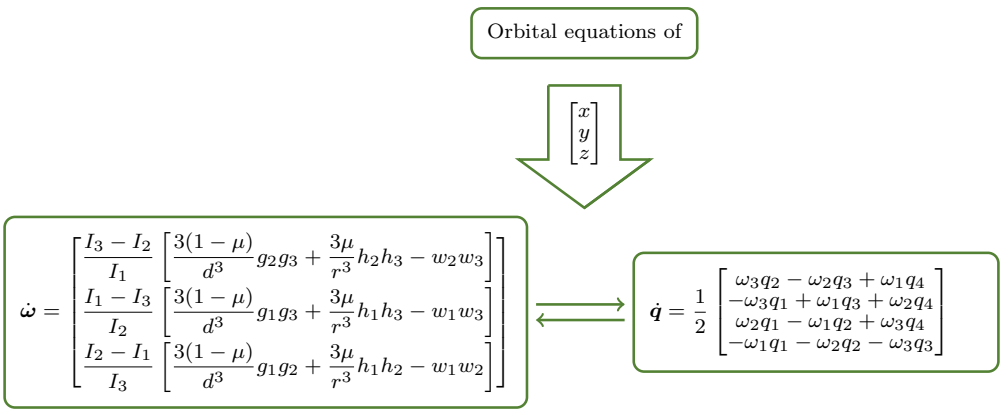

Fig. 2 Satellite's attitude dynamics equations in the P-CRTBP.

6.1 STM of SCM system of equations, $\mathrm{STM_{OA}}$

The STM of Eq. (9) is described as Eq. (10), where $\boldsymbol{J}_{\mathrm{OA}}$ is the Jacobian of the SCM system equations.

$$\begin{cases} \dot{\boldsymbol{\Phi}}_{\mathrm{OA}}(t,0) = \boldsymbol{J}_{\mathrm{OA}}(t)\boldsymbol{\Phi}_{\mathrm{OA}} \\ \boldsymbol{\Phi}_{\mathrm{OA}}(0,0) = \boldsymbol{I}_{13\times 13} \end{cases} \tag{10}$$

$$\boldsymbol{J}_{\mathrm{OA}}(t) = \begin{bmatrix} \frac{\partial f_x}{\partial \boldsymbol{x}_{\mathrm{orb}}} & \frac{\partial f_x}{\partial \boldsymbol{q}} & \frac{\partial f_x}{\partial \boldsymbol{\omega}} \\ \frac{\partial f_q}{\partial \boldsymbol{x}_{\mathrm{orb}}} & \frac{\partial f_q}{\partial \boldsymbol{q}} & \frac{\partial f_q}{\partial \boldsymbol{\omega}} \\ \frac{\partial f_\omega}{\partial \boldsymbol{x}_{\mathrm{orb}}} & \frac{\partial f_\omega}{\partial \boldsymbol{q}} & \frac{\partial f_\omega}{\partial \boldsymbol{\omega}} \end{bmatrix} \tag{11}$$

$\mathrm{STM_{OA}}$ is a 13 × 13 matrix demonstrating a linear mapping between a variation of the initial state and a variation of the final state. It is necessary to solve these 169 equations along with 13 governing equations of the SCM model to form $\mathrm{STM_{OA}}$. The quaternion vector elements must meet the constraint in Eq. (12):

$$q_1^2 + q_2^2 + q_3^2 + q_4^2 = 1 \tag{12}$$

To remove the sign ambiguity of q_4 and also avoid attributing a complex number, the infinitesimal variation of q_4 according to Eq. (12) will first be written as Eq. (13):

$$q_4\delta q_4 = -q_1\delta q_1 - q_2\delta q_2 - q_3\delta q_3 \tag{13}$$

From the previous equation,

$$\frac{\partial q_4}{\partial q_j} = -\frac{q_j}{q_4} \text{ for } j = 1,2,3 \tag{14}$$

Because q_4 is an autonomous variable, the partials of $\boldsymbol{J}_{\mathrm{OA}}$ relative to the first three components of the quaternion vector can be rewritten as Eq. (15):

$$\frac{\mathrm{d}\boldsymbol{f}(q_j,\omega_j)}{\mathrm{d}q_j} = \frac{\partial \boldsymbol{f}}{\partial q_j} + \frac{\partial \boldsymbol{f}}{\partial q_j}\frac{\partial q_4}{\partial q_j} \tag{15}$$

By applying the mentioned process, q_4 becomes an autonomous parameter. Thus, no partial derivative of the equations of motion concerning q_4 is essential to construct the Jacobian matrix. The differential equation for $\dot{q}_4$ is then left out throughout the scheming of $\boldsymbol{J}_{\mathrm{OA}}$. Thus, Jacobian matrix $\boldsymbol{J}_{\mathrm{OA}}$ of the SCM is converted into a 12 × 12 matrix, and the governing equations of $\mathrm{STM_{OA}}$ will decrease from 13 + 169 to merely 13 + 144 equations.

Then, $\mathrm{STM_{OA}}$ is updated to a new configuration ($\overline{\boldsymbol{\Phi}}_{\mathrm{OA}}$) as Eq. (16):

$$\begin{cases} \dot{\overline{\boldsymbol{\Phi}}}_{\mathrm{OA}}(t,0) = \overline{\boldsymbol{J}}_{\mathrm{OA}}(t)\overline{\boldsymbol{\Phi}}_{\mathrm{OA}} \\ \overline{\boldsymbol{\Phi}}_{\mathrm{OA}}(0,0) = \boldsymbol{I}_{12\times 12} \end{cases} \tag{16}$$

The final format for $\mathrm{STM_{OA}}$ is rewritten as Eq. (17):

$$\overline{\boldsymbol{\Phi}}_{\mathrm{OA}}(t_{\mathrm{f}},0) = \begin{bmatrix} \overline{\boldsymbol{\Phi}}_{\mathrm{OA}_{\boldsymbol{xx}}} & \overline{\boldsymbol{\Phi}}_{\mathrm{OA}_{\boldsymbol{xq}}} & \overline{\boldsymbol{\Phi}}_{\mathrm{OA}_{\boldsymbol{x\omega}}} \\ \overline{\boldsymbol{\Phi}}_{\mathrm{OA}_{\boldsymbol{qx}}} & \overline{\boldsymbol{\Phi}}_{\mathrm{OA}_{\boldsymbol{qq}}} & \overline{\boldsymbol{\Phi}}_{\mathrm{OA}_{\boldsymbol{q\omega}}} \\ \overline{\boldsymbol{\Phi}}_{\mathrm{OA}_{\boldsymbol{\omega x}}} & \overline{\boldsymbol{\Phi}}_{\mathrm{OA}_{\boldsymbol{\omega q}}} & \overline{\boldsymbol{\Phi}}_{\mathrm{OA}_{\boldsymbol{\omega\omega}}} \end{bmatrix} \tag{17}$$

6.2 SOAISC

The problem of calculating particular orbit–attitude responses was articulated as a more complex version of a simple root-finding problem by Guzzetti and Howell [15, 37]. In this paper, by exploiting state transition matrix $\mathrm{STM_{OA}}$, the SOAISC algorithm for the P-CRTBP is used for the convergence of the initial guess of the SCM state parameters to obtain accurate corrected initial conditions. Applying these initial conditions will result in periodic solutions. This correction algorithm may be distinguished from the correction algorithms developed in previous studies by its adaptation to the perturbed SCM equations. In fact, SOAISC is compatible with orbit–attitude equations for the perturbations of oblate and radiative planets. SOAISC combines a multi-variable Newton–Raphson with a single shooting method to detect particular initial conditions. Here the refined, corrected initial condition and initial guess vectors of the perturbed coupled orbit–attitude model are rendered by ς_0^* and ς_0, respectively. The correction process for the SOAISC is summarized in Fig. 3.

As previously mentioned, the proposed SOAISC algorithm needs an applicable initial guess as an input. The initial guess vector encompasses the initial guesses for both the orbit and attitude states. An appropriate initial guess vector for the orbital states can be appointed contiguous to the periodic orbit's initial conditions from the POC algorithm. Suitable initial guesses for the attitude states were made using the Poincaré mapping and Floquet theory methods.

7 Initial guess via Floquet theory

In the P-CRTBP, when the initial and final (after a period) orbital and attitude state variables are the same in the rotating frame, the value of the state variables is called a periodic solution. This periodic solution is a valuable tool that benefits from inherent features of the problem dynamics and shows states in which the attitude-behavior of the space vehicle can stay bounded after an adequate amount of time.

The process of finding periodic orbit and attitude solutions for different models within the three-body problem has two main parts. First, initial guesses need to be identified. Then, these initial guesses have to be refined through correction algorithms. The success of a correction algorithm dramatically depends on the relative accuracy

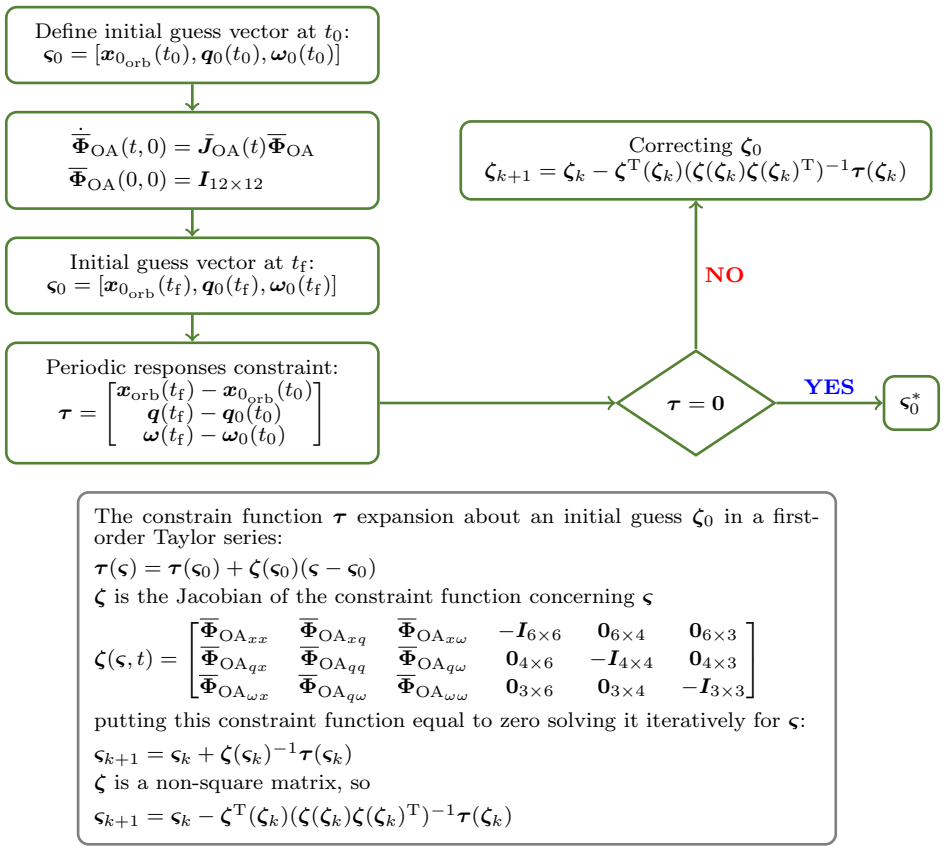

Fig. 3 SOAISC algorithm.

of the initial guesses. This is because these problems are highly nonlinear, and slight changes in the initial conditions could considerably change the final response.

In this research, two different methods were used to find the initial conditions for the periodic solution's correction algorithm. Two different approaches were used because the answers obtained varied as a result of these two methods using different hypotheses and attitude structures. On the other hand, any of these methods could be used to examine the attitude of a space vehicle along a periodic orbit because these methods illustrated the attitude behavior of the space vehicle differently. Specifically, this section explains how the initial guesses were made using the Floquet theory for the P-CRTBP. It should be noted that finding initial guesses for the coupled periodic solution in the U-CRTBP framework via the Floquet theory has been done before [30].

Initially, elementary solutions along periodic orbits are considered as references for investigating stability structures. As we already derived families of periodic orbits in the P-CRTBP, there are general attitude motions for an axisymmetric spacecraft, in which the attitude dynamics of the spacecraft remain unchanged for an observer in a rotating frame along these orbits. Considering an axisymmetric configuration can simplify the procedure of finding periodic solutions, and it is also a common configuration for space vehicles. In this research, $\hat{b}_3$ is regarded as a symmetry axis. Thus, the principal axes of moments of inertia along $\hat{b}_1$ and $\hat{b}_2$ are equal ($I_1 = I_2$). Therefore, the spacecraft mass distribution is exclusively described by the inertia ratio (K'), which varies between 0 and 1.

$$K' = \begin{cases} \frac{I_3 - I_1}{I_3}(\text{disk-like} \Rightarrow I_3 > I_1), & K \leqslant 0.5 \\ \frac{I_1 - I_3}{I_1}(\text{rod-like} \Rightarrow I_1 > I_3), & K > 0.5 \end{cases} \tag{18}$$

Elementary reference solutions are simple rotational motions. The initial attitude configuration of the spacecraft (resulting in nominal motions) is assumed to be $({}^{\rm i}\boldsymbol{q}^{\rm b}(t_0) = {}^{\rm r}\boldsymbol{q}^{\rm b}(t_0) = [0;0;0;1])$. This means that the spacecraft body axes coincide with the rotating frame axes. The angular velocity is assumed to be $({}^{\rm i}\boldsymbol{\omega}^{\rm b}(t_0) = [0;0;1])$. Based on these assumptions, as previously mentioned, the spacecraft attitude propagations seem

unchanged relative to the rotating frame because the angular velocity about $\hat{b}_3$ is considered to be 1 (ndim), which is the angular velocity of the primaries about the barycenter of the system. Because the spacecraft is axisymmetric, $\dot{\omega}_3$ is zero, and for elementary solutions, ω_2 and ω_1 are assumed to be zero. The new family of periodic orbits can be identified by all these assumptions and by the mean of the Floquet theory.

The Floquet theory uses a linear approximation of the stable structure of the space vehicle's elementary reference solution and a family of periodic orbits to identify the stability structure and its changes along with the family of orbits. These changes may reveal a new group of coupled periodic solutions. The stability structure of these periodic solutions is identified via eigenvalues ($\boldsymbol{\lambda}_i$) of the state transition matrix of SCM, $\mathrm{STM_{OA}}$, specifically, the eigenvalues of the attitude parts of general $\mathrm{STM_{OA}}$, $\overline{\boldsymbol{\Phi}}_{\mathrm{A}}$.

$$\overline{\boldsymbol{\Phi}}_{\mathrm{A}} = \begin{bmatrix} \overline{\boldsymbol{\Phi}}_{\mathrm{OA}_{qq}} & \overline{\boldsymbol{\Phi}}_{\mathrm{OA}_{q\omega}} \\ \overline{\boldsymbol{\Phi}}_{\mathrm{OA}_{\omega q}} & \overline{\boldsymbol{\Phi}}_{\mathrm{OA}_{\omega\omega}} \end{bmatrix} \tag{19}$$

Whenever the moduli of all the eigenvalues ($\boldsymbol{\lambda}_i$) of $\overline{\boldsymbol{\Phi}}_{\mathrm{A}}$ are lower than one, this shows linear stable modes for the reference periodic solution. Marginally linear stable modes are the states at which $|\boldsymbol{\lambda}_i| = 1$, and linear unstable modes are associated with $|\boldsymbol{\lambda}_i| > 1$. The SCM model formulation provides the ability to analyze just the rotational modes for the periodic reference solution, where changes in the attitude motions do not involve a variation of the spacecraft's orbital motion. On the other hand, the eigenvalues of $\overline{\boldsymbol{\Phi}}_{\mathrm{OA}}$ for the coupled problem are different from the eigenvalues associated with a pure attitude motion. This separation in the coupled and attitude modes is sensible because the monodromy matrix is a lower triangular block matrix [15, 30].

During the analysis of the stability structure of the periodic solutions and the family of orbits, the variation in the stability structure is evident. When the real components for one $\boldsymbol{\lambda}_i$ pair passes through the threshold, $|\boldsymbol{\lambda}_i| = 1$, the stability structure changes, which indicates a possible bifurcation of the periodic solutions. If the crossing occurs at $\boldsymbol{\lambda}_i = 1$, the change in stability is known as tangent bifurcation and may show a new group of periodic solutions in the vicinity of the reference with the same period. When the stability change along the family occurs at $\boldsymbol{\lambda}_i = -1$, the dynamics may bifurcate to a new periodic solution with twice the reference period, denoted as period-doubling bifurcation. Tangent and period-doubling bifurcations at an orbit–attitude reference solution can be identified by varying the reference trajectories across the selected family of periodic orbits and monitoring the real components of the eigenvalues for $\overline{\boldsymbol{\Phi}}_{\mathrm{A}}$.

8 Initial guess via Poincaré

Another powerful tool for constructing appropriate initial guesses for the periodic solution of the coupled orbit–attitude dynamic in the P-CRTBP is Poincaré sections. Poincaré maps are appreciated tools for capturing the structures of high-dimensional problem dynamics, such as the coupled P-CRTBP, by a discrete and lower-dimensional indication of the dynamical flow. The approach was employed to recognize coupled periodic solutions in the CRTBP [15]. The adaptation required in the P-CRTBP is employing extracted orbits within the model for reference orbital motions. This study used the Poincaré search method to identify initial guesses of coupled orbit–attitude periodic behaviors in the P-CRTBP for an axisymmetric space vehicle. The process of finding initial guesses via the Poincaré method for the P-CRTBP is described as designing a cross-section transverse to the dynamical flow, then setting a collection of initial conditions on the cross-section and propagating the underlying conditions for numerous rebounds to the section. A periodic solution could be identified by marking the rebounds to the cross-section. Crossings of an orbit path with the selected cross-section can be captured in terms of the desired state variables at the crossing. When two variables are chosen, each rebounding on the map is depicted by a spot in a plane that is transversal to the dynamical flow. A two-dimensional plot is adequate to recognize desirable dynamical structures. For example, the x–z plane could be selected as the transversal cross-section considering a planar orbit. Figure 4 presents a schematic of the Poincaré mapping method mechanism.

This study proposed initial alignments for the spacecraft body axes of ${}^{\mathrm{r}}\boldsymbol{q}^{\mathrm{b}}(t_0) = [0.7071; 0; 0; 0.7071]$ for a disk-shaped satellite and ${}^{\mathrm{r}}\boldsymbol{q}^{\mathrm{b}}(t_0) = [0.5; 0.5; 0.5; 0.5]$ for a rod-shaped satellite to meet the periodic responses of a simple coupled model. For both the rod-like and disk-like configurations, the space vehicle $\hat{\boldsymbol{y}}$ axis was considered to be orthogonal to the orbital plane to find new groups of initial guesses different from those found using the Floquet theory. Figure 5 shows the recorded q_2

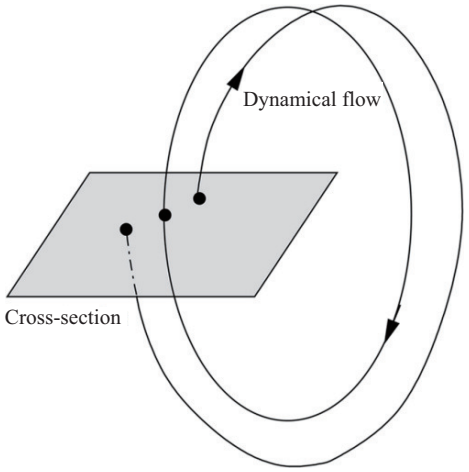

Fig. 4 Schematic of Poincaré mapping [40].

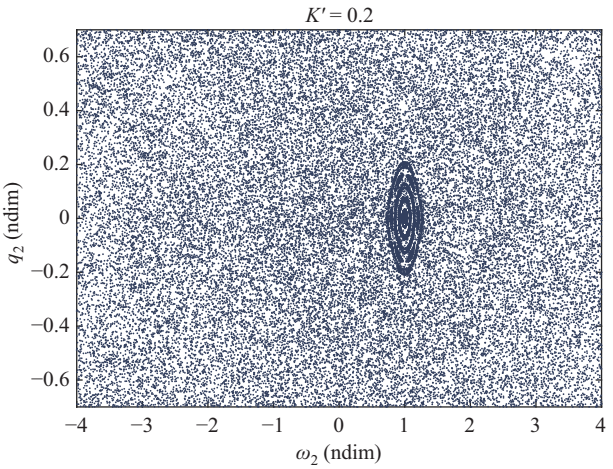

Fig. 5 Poincaré map with an island.

and ω_2 of a disk-shaped satellite with $K' = 0.2$ traveling in orbit with $T = 4.45$ around L_1 for 600 revolutions. After each period, the orbital state variables are refreshed to preserve the periodicity. Closed curves called islands in the Poincaré map render bounded behaviors and periodic solutions, as represented in Fig. 5.

This means that a particular value for the angular velocity in the initial conditions for the coupled dynamic will produce periodicity for a specific kind of orbit. The chaotic dynamical behavior of the coupled P-CRTBP is evident from Poincaré maps; nevertheless, bounded performances are portions of the general response. In this study, this approach, in combination with the Floquet theory, was used to discover initial guesses for the periodic attitude motions of a space vehicle with an axisymmetric configuration; however, the attitude-behavior of the spacecraft was regarded in all three dimensions. The flowchart in Fig. 6 shows the procedure for obtaining precise coupled periodic solutions.

9 Results

In this paper, it is assumed that the Sun is the largest primary and is radiative, and the Earth is a smaller and oblate primary, as represented by m_1 and m_2, respectively. Table 1 lists the constant values in this system, where $\mu_{\text{Sun–Earth}}$ is the mass ratio of the Sun–Earth system, $D_{\text{Sun–Earth}}$ is the distance between the Sun and the Earth, $T_{\text{Sun–Earth}}$ is the orbital period of the Earth around the Sun, $J_2^{(\text{Earth})}$ is the oblateness parameter of the Earth, R_{e} is the Earth's equatorial radius, and q is the mass reduction factor of the Sun.

When initial guess vector $\boldsymbol{\varsigma}_0$ has the proper level of precision, the probability of attaining more truthful initial values, $\boldsymbol{\varsigma}_0^*$, increases, which leads to coupled periodic

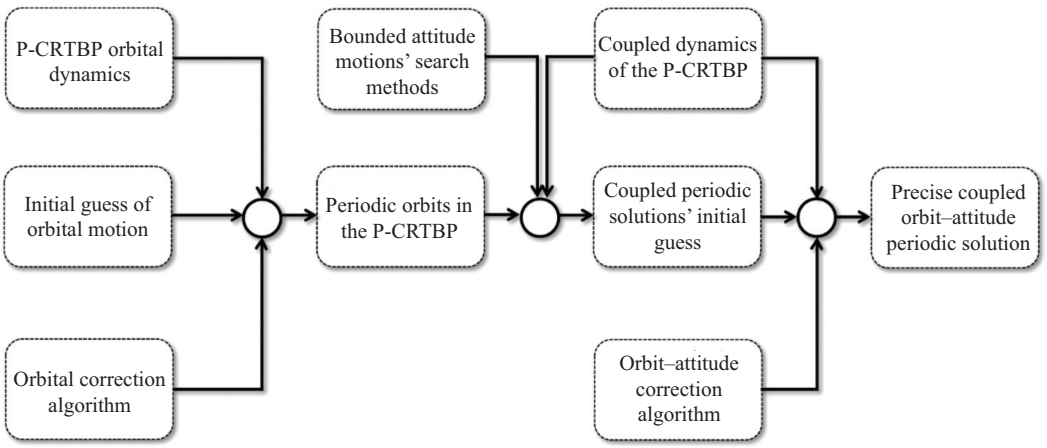

Fig. 6 Problem flowchart.

Table 1 Perturbed constants of Sun–Earth system

$\mu_{\text{Sun–Earth}}$	3×10^{-6}
$D_{\text{Sun–Earth}}$ (km)	151.89×10^{6}
$T_{\text{Sun–Earth}}$ (d)	365.256
$J_2^{(\text{Earth})}$	1.0826×10^{-3}
R_{e} (km)	6378.1
q	0.99934

solutions for the P-CRTBP. As previously stated, an excellent initial guess vector for the orbital states can be selected from the periodic orbit's initial conditions extracted from the POC algorithm. POC receives an initial guess around the libration point and propagates it to achieve initial conditions for all the periodic orbits in the family of orbits under consideration. The initial guess for each family may be selected from the known orbits in the U-CRTBP [8, 24, 33, 37, 41, 42] around a specific libration point. The results showed the ability of the POC algorithm to obtain more than 2000 periodic orbits with different periods for each family. Tables 2 and 3 list some of the refined initial conditions for the P-CRTBP of the periodic orbits, which are known as the reference trajectories of the coupled model around the collinear libration points. In this study, for the ath orbit around collinear equilibrium point c, the Lyapunov and Halo families are found using $L(c{:}a)$ and $H(c{:}a)$, respectively. The resemblance between the P-CRTBP periodic orbits presented in Figs. 7 and 8 and the U-CRTBP solutions found in the literature [8, 24, 33, 37, 41, 42] can be considered as a logical validation of the acquired answers, as seen in Table 2.

In this article, as reference trajectories, the Lyapunov orbits around the L_1 and L_2 libration points are considered to be the basis of extracting coupled periodic solutions. Because periodic orbital responses are dependent on a system's parameters, it is necessary to study the effect of perturbations on them. The differences between the periodic orbit initial conditions of the two U-CRTBP and P-CRTBP models are shown in Fig. 9 for the same initial guess vectors for the Lyapunov families around L_1 and L_2.

It can be seen that by increasing the period time, the difference between the periodic orbit initial conditions of the U-CRTBP and P-CRTBP models will first decrease and then increase. According to Fig. 9, the delta values are small and may seem unimportant, but Fig. 10 shows that the perturbed case breaks out from the periodic shape and diverges in the Lyapunov families of orbits

Table 2 Some of the extracted P-CRTBP's Lyapunov periodic orbits propagated via the proposed POC algorithm

	x_0 (ndim)	y_0 (ndim)	z_0 (ndim)	v_{x_0} (ndim)	v_{y_0} (ndim)	v_{z_0} (ndim)	T (ndim)
Initial guess Lyapunov L_1	0.980000	0	0	0	0.004000	0	3.0000
Correction L(1:1)	0.989386	0	0	0	0.004629	0	3.0240
Propagate L(1:10)	0.988921	0	0	0	3.056000	0	3.0560
Propagate L(1:100)	0.987672	0	0	0	0.020478	0	3.4160
Propagate L(1:220)	0.986786	0	0	0	0.025756	0	3.8960
Initial guess Lyapunov L_2	1.010000	0	0	0	−0.005000	0	3.0100
Correction L(2:1)	1.010767	0	0	0	−0.005194	0	3.0696
Propagate L(2:100)	1.012462	0	0	0	−0.020692	0	3.4616
Propagate L(2:400)	1.014874	0	0	0	−0.030293	0	4.6616
Propagate L(2:480)	1.015659	0	0	0	−0.031958	0	3.9815

Table 3 Some of the extracted P-CRTBP's Halo periodic orbits propagated via the proposed POC algorithm

	x_0 (ndim)	y_0 (ndim)	z_0 (ndim)	v_{x_0} (ndim)	v_{y_0} (ndim)	v_{z_0} (ndim)	T (ndim)
Initial guess Halo L_1	0.9850000	0	0.0170000	0	−0.006000	0	2.3200
Correction H(1:1)	0.9988990	0	0.0188880	0	−0.006868	0	2.3560
Propagate H(1:10)	0.9993390	0	0.0205425	0	−0.007070	0	2.3710
Propagate H(1:100)	1.0002126	0	0.0300000	0	−0.006000	0	2.8560
Propagate H(1:220)	1.0000800	0	0.0456300	0	−0.005150	0	3.0060
Initial guess Halo L_2	1.0010000	0	0.0110000	0	−0.004000	0	1.2000
Correction H(2:1)	1.0014010	0	0.0112500	0	−0.004200	0	1.4000
Propagate H(2:100)	1.0037000	0	0.0119000	0	−0.009400	0	1.7500
Propagate H(2:400)	1.0092000	0	0.0096000	0	−0.014790	0	2.8890
Propagate H(2:480)	1.0100300	0	0.0077000	0	−0.013700	0	2.9900

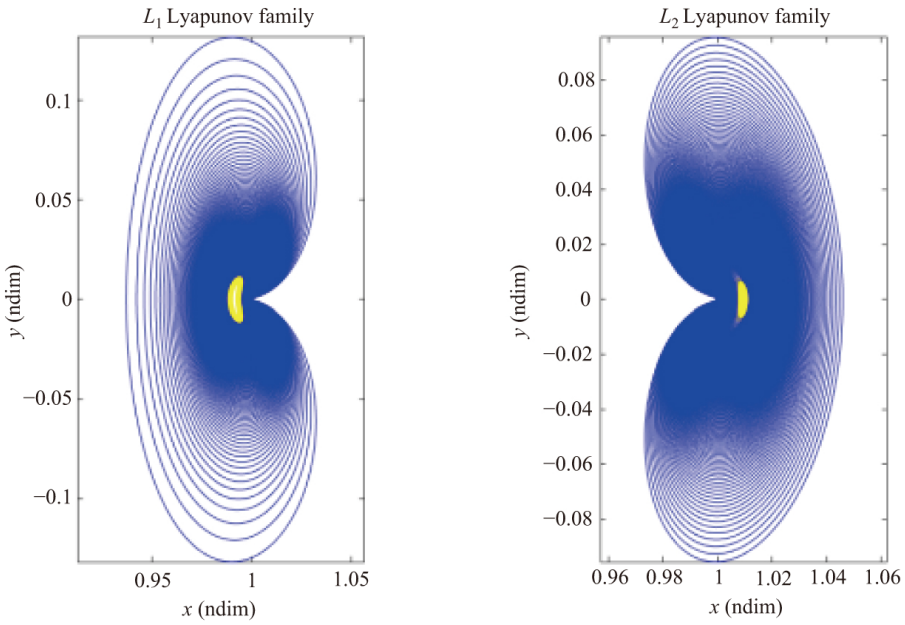

Fig. 7 P-CRTBP Lyapunov families of orbits around L_1 and L_2, where each family's first orbit is shown in yellow.

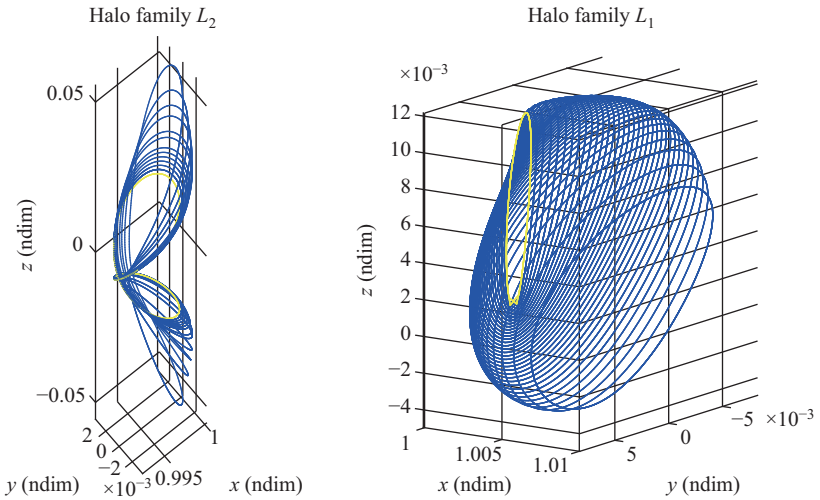

Fig. 8 P-CRTBP Halo families of orbits around L_1 and L_2, where each family's first orbit is shown in yellow.

around L_1 and L_2. It should be noted that this issue is true in all of the orbits of these families.

In general, the problem may have several periodic or quasi-periodic and non-periodic responses. Therefore, to find periodic solutions, the problem needs appropriate initial conditions. In this study, the SOAISC algorithm was proposed to modify and obtain these initial conditions. However, the periodic solutions are restricted, and a good initial guess vector, ς_0, will raise the probability of finding precise initial conditions, ς_0^*. An initial guess is suggested by employing orbital states close to a periodic orbit's corrected initial conditions, as listed in Table 2 and based on the Poincaré mapping or Floquet theory. In Section 8, appropriate spacecraft configurations were identified using the Poincaré mapping and Floquet theory. In the following, an example of recognizing the appropriate initial guess for ω_{2_0} is given for an Lyapunov orbit of the P-CRTBP about the L_1 point. The Poincaré map of angular velocity ω_{2_0} and quaternion q_{2_0} is shown in Fig. 11. The island centers that emerge on this map are appropriate initial guesses.

Each island that appears on the map may result in periodic solutions for the perturbed coupled model. For instance, Table 4 lists some periodic responses when

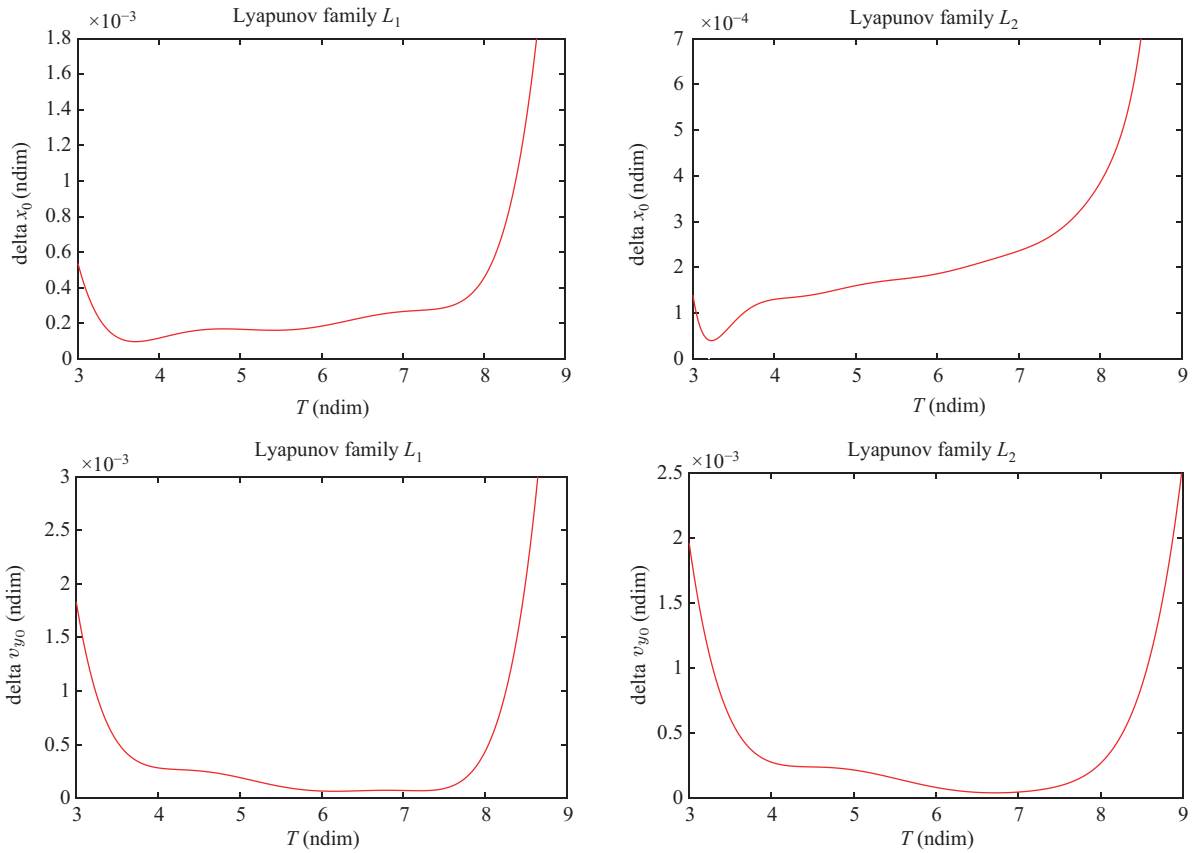

Fig. 9 Difference between the initial conditions of U-CRTBP and P-CRTBP periodic orbits (delta x_0, delta v_{y_0}) for the same initial guess vectors of the Lyapunov families of orbits around L_1 and L_2.

Table 4 Correction of coupled periodic P-CRTBP initial guess vectors for the island centers that emerged in Fig. 11

Orbit	x_0 (ndim)	v_{y_0} (ndim)	q_{1_0} (ndim)	q_{2_0} (ndim)	q_{3_0} (ndim)	q_{4_0} (ndim)	ω_{1_0} (ndim)	ω_{2_0} (ndim)	ω_{3_0} (ndim)	T (ndim)
$\varsigma_0(L(1{:}1))$	0.98000000	0.01900000	0.7071000	0	0	0.7071000	0	1	0	3.4415
$\varsigma_0^*(L(1{:}1))$	0.98753688	0.02032653	0.7070159	0	0	0.7071076	−0.0000001	1	0.0000002	
$\varsigma_0(L(1{:}1))$	0.98000000	0.01900000	0.7071000	0	0	0.7071000	0	−2.8000	0	3.4415
$\varsigma_0^*(L(1{:}1))$	0.98753688	0.02032653	0.7070950	0.0007	0.0012	0.7071170	−0.0018	−2.6684	−0.000006	

choosing a ω_{2_0} value equal to 1 (ndim) or −2.8 (ndim) for the island centers that emerged in Fig. 11.

An important factors in the process of obtaining periodic responses is inertia ratio K'. Thus, to find the appropriate range for K', periodic P-CRTBP orbits were examined for several values of K'. The results for the first and third orbits of the L_2 Lyapunov family ($L(2{:}1)$ and $L(2{:}3)$) are illustrated in Fig. 12.

Based on the number of islands on the Poincaré map, increasing the inertia ratio decreases the chance of finding periodic responses. On the other hand, an orbit with a shorter period is more favorable for periodic responses for the same value of K' in each family. Figure 12 indicates that there are more periodic solutions for a spacecraft with a lower inertia ratio traveling in an orbit with a shorter orbital period.

More importantly, the effect of perturbations on the coupled orbit–attitude behavior can be expressed by comparing Poincaré maps of the U-CRTPB and P-CRTBP models with the same initial guess vector. Figure 13 compares Poincaré maps of a disk-shaped satellite with $K' = 0.05$ revolving in the first orbit of the L_1 Lyapunov family in the Sun–Earth system for two different models.

The changes in the patterns that appear on the Poincaré map are caused by the addition of perturbations

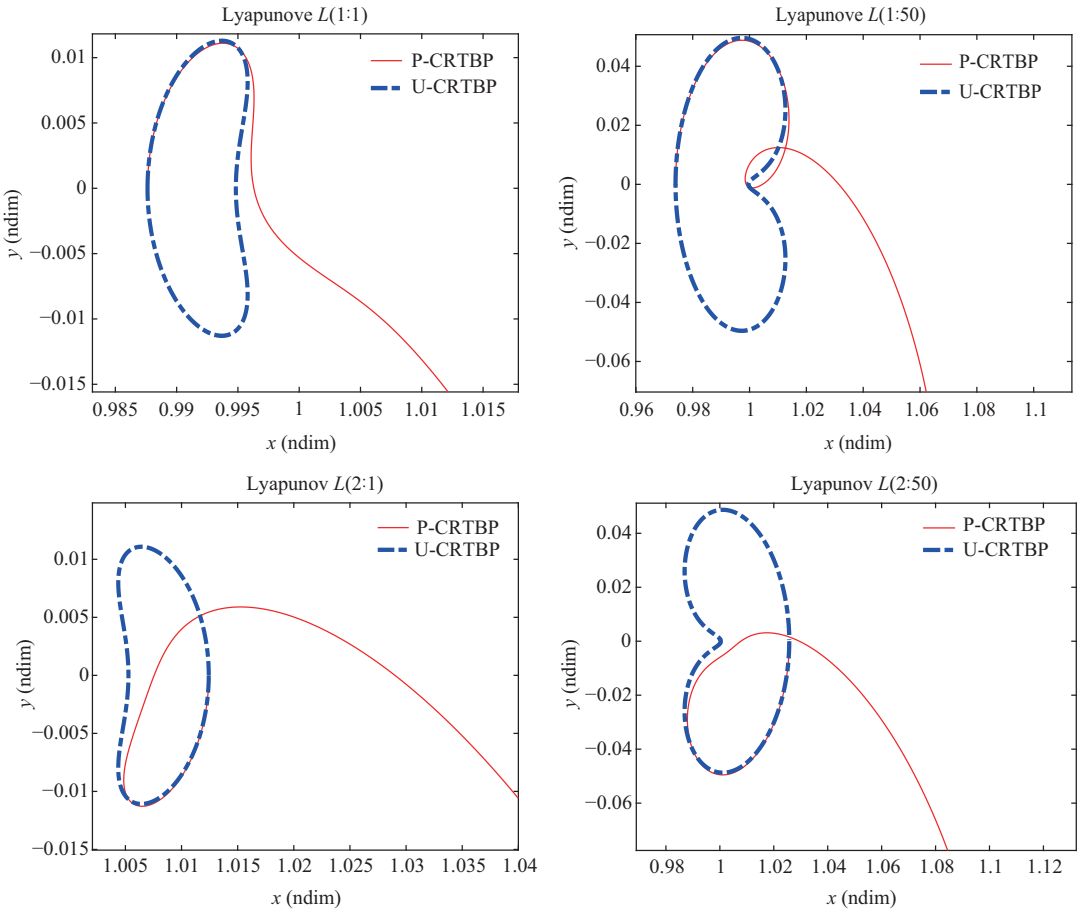

Fig. 10 Applying the orbital initial conditions of the U-CRTBP to P-CRTBP. The perturbed case breaks out from the periodic shape and diverges in the Lyapunov families of orbits around L_1 and L_2.

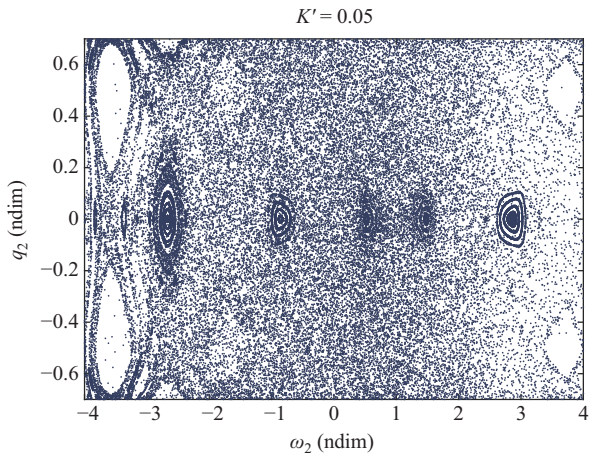

Fig. 11 Poincaré map for an L_1 Lyapunov orbit (the first orbit of the family) in the Sun–Earth system for a spacecraft with $K' = 0.05$.

to the problem. The shifting of the island centers that emerge in the perturbed model compared to the unperturbed model causes the selection of different values for the attitude states of the perturbed vs. unperturbed coupled model as the input of the SOAISC correction algorithm.

The research conducted in this study suggested that employing the angular velocity vector as $[0, \omega_{2_0}, 0]$ (the value of ω_{2_0} obtained from the island centers that emerge on the Poincaré map) for the corresponding part of the initial guess vector is usually a suitable initial guess. Table 5 explains that the reference trajectory is directly influenced by the perturbation of the Sun's radiation pressure and the Earth's oblateness and indirectly affects the attitude dynamics.

Various sets of periodic attitude motions within the P-CRTBP can be discovered using other search methods to complement the solution space. The identification of new groups of coupled periodic solutions using the Floquet theory method can be summarized as follows.

(1) A graph of the stability index (S) for different inertia ratios along a family of orbits is constructed.

(2) The regions with changes in the stability structure are identified as initial guesses for the correction algorithm.

(3) The identified values are corrected via a correction algorithm to extract precise orbit–attitude periodic solutions for the P-CRTBP.

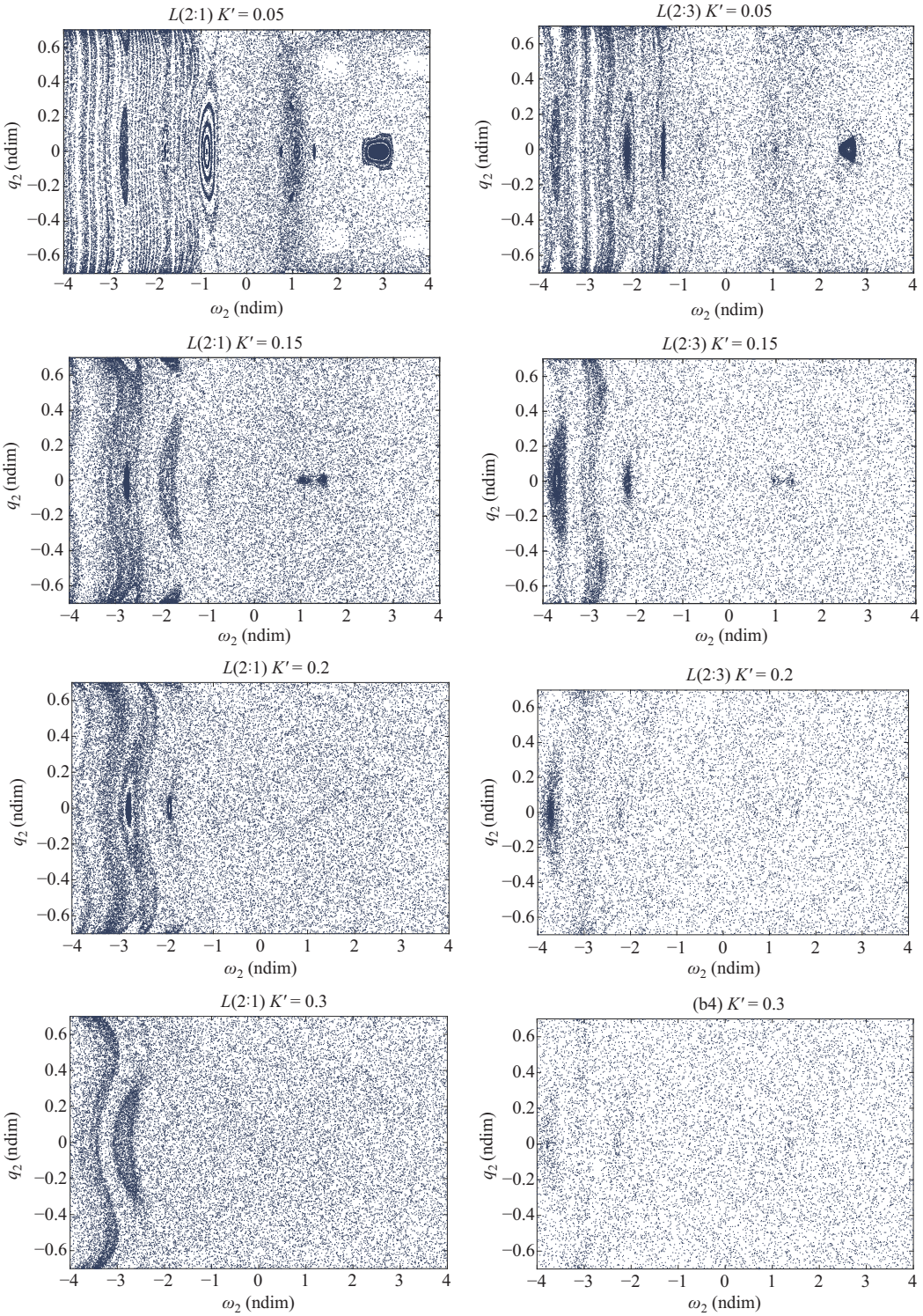

Fig. 12 First and third orbits of the P-CRTBP L_2 Lyapunov family were examined for several values of K' with the same orbit.

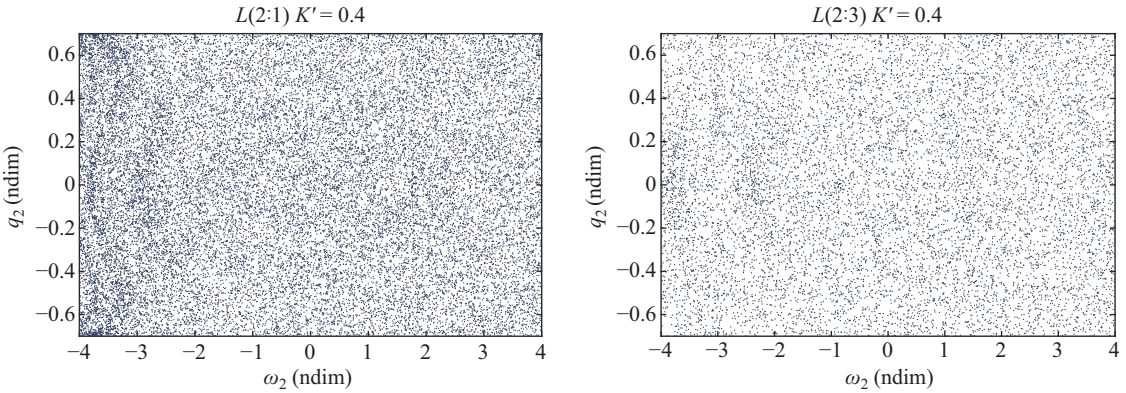

Fig. 12 (Continued)

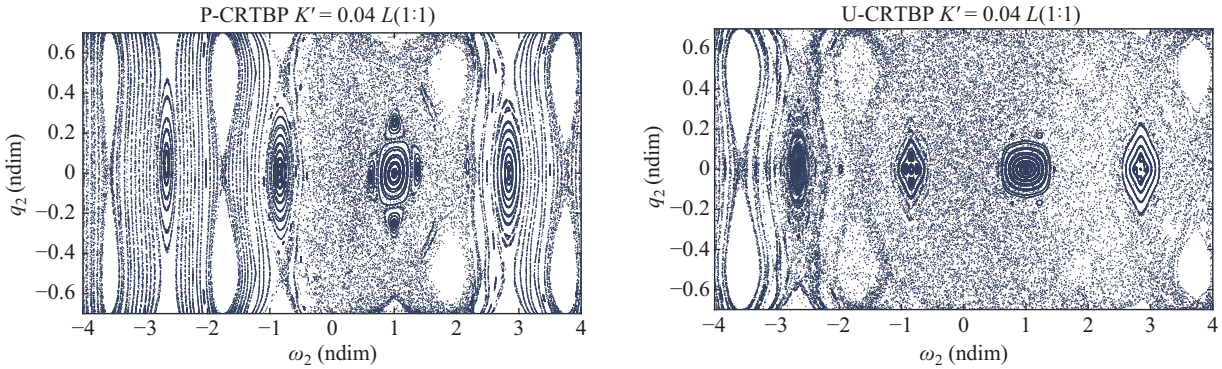

Fig. 13 Poincaré maps of the P-CRTBP and U-CRTBP models with the same initial guess vector.

Table 5 Some of P-CRTBP and U-CRTBP coupled periodic corrected initial conditions for the Sun–Earth system with Lyapunov reference trajectories around the L_1 and L_2 libration points, which are denoted by $\varsigma_0^{*\mathrm{P}}$ and $\varsigma_0^{*\mathrm{U}}$, respectively, for the same initial guess vector, ς_0, for a satellite with $K' = 0.2$

	x_0 (ndim)	v_{y_0} (ndim)	q_{1_0} (ndim)	q_{2_0} (ndim)	q_{3_0} (ndim)	q_{4_0} (ndim)	ω_{1_0} (ndim)	ω_{2_0} (ndim)	ω_{3_0} (ndim)	T (ndim)
ς_0	0.98000000	0.01900000	0.707100	0	0	0.7071000	0	1	0	3.4415
$\varsigma_0^{*\mathrm{P}}(L^{\mathrm{P}}(1{:}1))$	0.98753688	0.02032653	0.707100	0	0	0.7070159	−0.0000001	1	0.0000002	
$\varsigma_0^{*\mathrm{U}}(L^{\mathrm{U}}(1{:}1))$	0.98751234	0.02031022	0.706400	0	0	0.7078000	−0.0000012	1	0	
ς_0	1.010000	−0.010000	0.7071000	0	0	0.7071000	0	1	0	3.0900
$\varsigma_0^{*\mathrm{P}}(L^{\mathrm{P}}(2{:}1))$	1.01126000	−0.010169	0.707104	0	0	0.7141000	0.00002	1	0.000001	
$\varsigma_0^{*\mathrm{U}}(L^{\mathrm{U}}(2{:}1))$	1.01123200	−0.010111	0.706600	0.0002	0.0005	0.6929000	0	1.01	0	

The stability index is defined as Eq. (20) to illustrate the stability structure according to the elementary reference periodic response:

$$S = \frac{1}{2}\left(\lambda_{\max} + \frac{1}{\lambda_{\max}}\right) \tag{20}$$

where $\lambda_{\max} = \max|\boldsymbol{\lambda}_i|$ represents the value of the supreme eigenvalue. A stability index of one indicates marginally stable behaviors, which correspond to a collection of quasi-periodic behaviors in the proximity of the reference solution. On the other hand, a stability index that is larger than one indicates unstable behavior in the region of the reference. A higher stability index corresponds to a quicker divergence from the reference. The stability index comprehensively represents how the stability structure changes when the reference orbit and inertia ratio change.

Figure 14 illustrates stability indexes for a disk-shaped satellite in nominal motion in the P-CRTBP and U-CRTBP. The disk-shaped configuration shows a larger diversity for the stability structure, which corresponds to

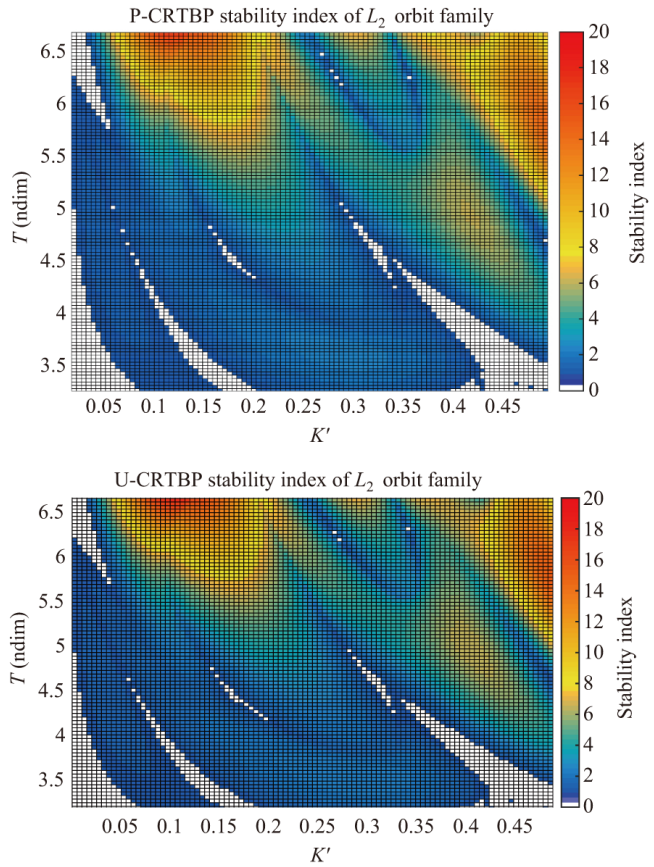

Fig. 14 Stability index representation of a disk-like spacecraft in reference motion for two different models (P-CRTBP and U-CRTBP) of the three-body problem.

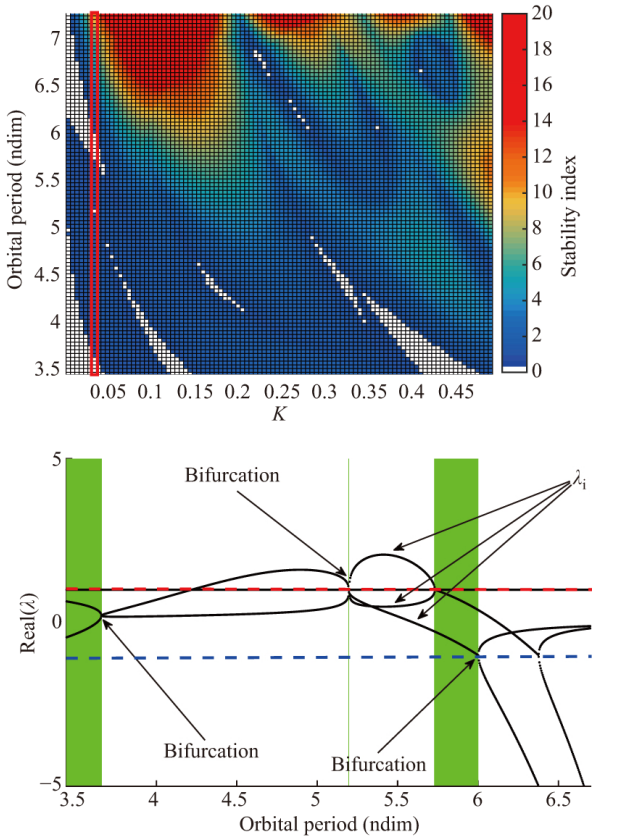

Fig. 15 The upper figure shows a disk-like spacecraft's stability index and the family of Lyapunov orbits around L_1 in the P-CRTBP. The bottom figure shows the corresponding eigenvalue propagation by the red narrow rectangular boxes. The green areas in the right figure show regions where the stability index is equal to one, while the white areas show regions where the stability index is greater than one.

more bifurcations of periodic solutions. Nominal motions that are stable are more common for orbits with shorter periods, while the instability of the reference solution becomes prevalent as the orbital period becomes longer, and the orbit gets closer to the primaries. As expected, the figure shows almost similar stability structures for the U-CRTBP and P-CRTBP in the nominal motions. Because of the assumptions of the Floquet theory, this method cannot be an appropriate means to perform a comparative assessment of different models, but it can still be used to provide suitable initial guesses. On the other hand, rod-shaped configurations are unstable, and there is no bifurcation of the periodic solution in the stability index. A larger orbit and inertia ratio yield faster divergences for both disk-shaped and rod-shaped space vehicles, which is represented by a higher stability index.

Figure 15 shows the stability index values for a disk-like spacecraft for the family of Lyapunov orbits around L_1 in the P-CRTBP. A narrow red rectangular in the figure marks the stability index for a spacecraft with $K' = 0.035$ along with the family of orbits around L_1. The corresponding eigenvalue evolution of the marked region in the right-hand plot of Fig. 13 is illustrated in the left-hand plot of Fig. 13. The locations of bifurcations of new groups of periodic solutions are shown in this figure, and these values with slight modifications are employed as initial guesses for the correction algorithm. Eq. (21) defines the process of evaluating the initial guesses.

$$\begin{bmatrix} {}^{\mathrm{r}}\boldsymbol{q}^{\mathrm{b}}(\mathbf{0}) \\ {}^{\mathrm{r}}\dot{\boldsymbol{\omega}}^{\mathrm{b}}(\mathbf{0}) \end{bmatrix}_{\text{Initial Guess}} = \begin{bmatrix} {}^{\mathrm{r}}\boldsymbol{q}^{\mathrm{b}}(\mathbf{0}) \\ {}^{\mathrm{r}}\dot{\boldsymbol{\omega}}^{\mathrm{b}}(\mathbf{0}) \end{bmatrix}_{\text{Reference}} + \epsilon\Lambda \tag{21}$$

Here, ϵ is an appropriate coefficient, and Λ is a linear combination of the real and imaginary parts for the eigenvectors associated with the stability crossing eigenvalues. Some of the refined periodic responses related to the same initial guesses obtained using the Floquet theory for the two models are listed in Table 6.

Table 6 Some of the P-CRTBP and U-CRTBP periodic coupled orbit–attitude corrected initial conditions obtained with the proposed SOAISC algorithm for the Sun–Earth system with Lyapunov reference trajectories around the L_1 and L_2 libration points, as denoted by $\varsigma_0^{*\mathrm{P}}$ and $\varsigma_0^{*\mathrm{U}}$, respectively, for the same initial guess vector, ς_0, for a satellite with $K' = 0.322$ for the first row and $K' = 0.435$ for the second row. The initial guess vector was selected using the Floquet theory. L^{P} and L^{U} show the Lyapunov trajectories of the perturbed and unperturbed models, respectively

	x_0 (ndim)	v_{y_0} (ndim)	q_{1_0} (ndim)	q_{2_0} (ndim)	q_{3_0} (ndim)	q_{4_0} (ndim)	ω_{1_0} (ndim)	ω_{2_0} (ndim)	ω_{3_0} (ndim)	T (ndim)
ς_0	0.98000000	0.02000000	0	0	0	1	0	0	1	4.529
$\varsigma_0^{*\mathrm{P}}(L^{\mathrm{P}}(1{:}350))$	0.98533135	0.02954547	0.82	0.17	0.29	0.47	0.59	0.21	0.59	
$\varsigma_0^{*\mathrm{U}}(L^{\mathrm{U}}(1{:}350))$	0.98547507	0.02977917	0	0	0.18	0.98	0	0	1	
ς_0	1.01200000	−0.0240000	0	0	0	1	0	0	1	3.769
$\varsigma_0^{*\mathrm{P}}(L^{\mathrm{P}}(2{:}55))$	1.01291430	−0.0247930	0	0	0.3357	0.94197	0	0	−0.53712	
$\varsigma_0^{*\mathrm{U}}(L^{\mathrm{U}}(2{:}55))$	1.01302930	−0.0244122	0	0	−0.2100	0.97000	0	0	1	

Aside from the different structures of the periodic motions (differences in the initial conditions) identified using the Floquet theory and Poincaré maps, some of the relevant issues are addressed in the presented results based on the Floquet theorys. For example, an elementary case is provided that works within the Floquet theory assumptions and may be used as a stepping stone to identifying more sophisticated and complex orbit–attitude periodic motions. The definitions of attitude modes that define nearby rotational behaviors, as well as the compact visualization of stability information across a vast range of specified parameters, are both aided by the analysis of the linear stability for an orbit–attitude nominal motion. On the other hand, Poincaré maps are another method for uncovering key dynamical features like periodic solutions. A simple approach for the automated recognition of structured patterns on the map is given to aid the assessment of multiple surfaces of sections, ones that may reflect a range of system configurations. The orbit–attitude dynamics within the P-CRTBP may be transferred to other applications using this method.

10 Conclusions

Periodic orbits and natural periodic orbit–attitude motions in the P-CRTBP were investigated by considering the perturbations of a radiated massive primary and an oblate secondary. The radiated massive primary was the Sun, and each of the solar system's planets could be considered as an oblate secondary. Because the problem has no closed-form solution, various numerical and search methods were used to achieve this aim. Thus, in this research, families of periodic planar orbits in the P-CRTBP with respect to a radiated primary and an oblate secondary were identified using the proposed algorithm. The derived orbits were a large part of the coupled problem solution. Then, using two separate search approaches, the attitude dynamics of a satellite traveling along recognized orbital motions were studied. Using two different search methods supplemented the solution space and provided insight into the attitude motions for space vehicles with different structures. It should also be noted that the influences of various space vehicle and model parameters were examined, after which natural accurate orbit–attitude periodic solutions were extracted and compared to those of the U-CRTBP.

The investigation revealed that the periodic solutions for the coupled orbit–attitude of the P-CRTBP relied on the three main parameters.

- The first was the reference orbit, which was affected by the perturbations in a straightforward manner. Because the attitude dynamics equations change with the reference orbit in the simplified coupled model, the attitude dynamics of a space vehicle are influenced by the perturbations.
- The second was selecting appropriate initial guesses for the angular velocities and spacecraft alignments. The initial guess vector of the angular velocity and quaternions was obtained using the search methods.
- The third was an inertia ratio assessment. Based on this value, the problem could have different periodic solutions or even no periodic response for different cases.

A comparison of the P-CRTBP and U-CRTBP coupled models demonstrated that considering the perturbations could result in a more realistic simulation of the research environment, which could yield a model that was much closer to real mission conditions.

Appendix A

A.1 Potential fields of primaries

The total gravitational potential field on a spacecraft equals the sum of the radiated and oblate primaries quota.

A.2 Potential field of oblate primary

The potential gravitational field of the oblate secondary m_2 can be written as Eq. (A1) [33]:

$$V(r,\varnothing)=-\frac{G}{r}\left[1-\sum_{k=1}^{\infty}J_{2k}\left(\frac{R}{r}\right)^{2K}P_{2k}(\cos\psi)\right] \tag{A1}$$

where J_{2k} is the $2k$th zonal harmonic of the oblate mass, R is the equatorial radius of the oblate body, P_{2k} is the legendre polynomial, and ψ is the angle between the polar axis of the primary and the vector from the center to a space vehicle at distance r [38]. Note that because J_2 is the largest zonal harmonic so far, this study focused only on its contribution to the gravitational perturbations. Then, the potential field due to the oblate mass in rendered in a non-dimensional form:

$$V_{\text{oblate}}=-\mu\left(\frac{1}{r}+\frac{A_2}{r^3}\right) \tag{A2}$$

The oblate coefficient is rendered by A_2 and equal to J_2R^2. In addition, R is recognized as the oblate body's equatorial radius, and r is the non-dimensional distance from m_2.

$$r=\sqrt{(x-1+\mu)^2+y^2+z^2} \tag{A3}$$

A.3 Potential field due to the Sun

It is assumed that the radiation force of the Sun is always applied to a spacecraft in the direction of its light. Thus, if this force is considered, the Sun's gravitational field should be modified, which causes a reduction of the Sun's mass [43]. The mass reduction factor can be calculated from Eq. (A4) [44]:

$$q=1-\frac{F_{\text{P}}}{F_{\text{g}}} \tag{A4}$$

where F_{P} and F_{g} represent the radiation force and gravitational force due to the Sun, respectively. The mass reduction factor, q, is considered constant if it is assumed that the radiation force always acts on a spacecraft away from the Sun in the line between the Sun and spacecraft [44]. After defining the mass reduction factor, the potential field due to the Sun can be expressed as Eq. (A5):

$$V_{\text{Sun}}=-(1-\mu)\left(\frac{q}{d}\right) \tag{A5}$$

where d is the non-dimensional distance from the Sun:

$$d=\sqrt{(x+\mu)^2+y^2+z^2} \tag{A6}$$

Finally, the potential field of the P-CRTBP could be explained as the sum of the portions of the individual primaries.

$$V=\left[-\mu\left(\frac{1}{r}+\frac{A_2}{r^3}\right)\right]+\left[-(1-\mu)\left(\frac{q}{d}\right)\right] \tag{A7}$$

A.4 Kinetic equation of the system

The kinetic energy of a space vehicle in a rotating frame is expressed as Eq. (A8) [44]:

$$K=\frac{1}{2}(v_x^2+v_y^2+v_z^2)+n(x\dot{y}-\dot{x}y)+\frac{1}{2}n^2(x^2+y^2) \tag{A8}$$

where the space vehicle's velocity components and the mean motion are represented by v_x, v_y, v_z, and n, respectively [12].

$$n=1+\frac{3}{2}A_2 \tag{A9}$$

Appendix B

$\boldsymbol{g}_i$ and $\boldsymbol{h}_i$ are the projections of the unit vectors of a space vehicle's positions relative to the Sun and an oblate body into the body frame, respectively [38, 39]:

$$\begin{cases}\begin{bmatrix}g_1\\g_2\\g_3\end{bmatrix}=\boldsymbol{A}_{\hat{b}.\hat{i}}\boldsymbol{A}_{\hat{i}.\hat{r}}\dfrac{\boldsymbol{d}}{d}=\boldsymbol{A}_{\hat{b}.\hat{i}}\boldsymbol{A}_{\hat{i}.\hat{r}}\dfrac{1}{d}\begin{bmatrix}x+\mu\\y\\z\end{bmatrix}\\ \begin{bmatrix}h_1\\h_2\\h_3\end{bmatrix}=\boldsymbol{A}_{\hat{b}.\hat{i}}\boldsymbol{A}_{\hat{i}.\hat{r}}\dfrac{\boldsymbol{r}}{r}=\boldsymbol{A}_{\hat{b}.\hat{i}}\boldsymbol{A}_{\hat{i}.\hat{r}}\dfrac{1}{d}\begin{bmatrix}x-1+\mu\\y\\z\end{bmatrix}\end{cases} \tag{B1}$$

$\boldsymbol{A}_{\hat{i}.\hat{r}}$ is the rotation matrix from the reference frame to the inertia frame [38, 39]:

$$\boldsymbol{A}_{\hat{i}.\hat{r}}=\begin{bmatrix}\cos t & -\sin t & 0\\ \sin t & \cos t & 0\\ 0 & 0 & 1\end{bmatrix} \tag{B2}$$

$\boldsymbol{A}_{\hat{b}.\hat{i}}$ is the direction cosine matrix corresponding to the quaternions vector [38, 39]:

$$\boldsymbol{A}_{\hat{b}.\hat{i}}=\begin{bmatrix}q_1^2-q_2^2-q_3^2+q_4^2 & 2(q_1q_2+q_3q_4) & 2(q_1q_3-q_2q_4)\\ 2(q_1q_2-q_3q_4) & -q_1^2+q_2^2-q_3^2+q_4^2 & 2(q_2q_3+q_1q_4)\\ 2(q_1q_3+q_2q_4) & 2(q_2q_3+q_1q_4) & -q_1^2-q_2^2+q_3^2+q_4^2\end{bmatrix} \tag{B3}$$

Declaration of competing interest

The authors have no competing interests to declare that are relevant to the content of this article.

References

[1] Wertz, J. R. *Spacecraft Attitude Determination and Control*. Springer Dordrecht, **1978**.

[2] Sidi, M. *Spacecraft Dynamics and Control: A Practical Engineering Approach*. Cambridge University Press, **1997**.

[3] Markley, F. L., Crassidis, J. L. *Fundamentals of Spacecraft Attitude Determination and Control*. Springer New York, **2014**.

[4] Wong, B., Patil, R., Misra, A. Attitude dynamics of rigid bodies in the vicinity of the Lagrangian points. *Journal of Guidance, Control, and Dynamics*, **2008**, 31(1): 252–256.

[5] Bakhtiari, M., Daneshjou, K., Abbasali, E. A new approach to derive a formation flying model in the presence of a perturbing body in inclined elliptical orbit: Relative hovering analysis. *Astrophysics and Space Science*, **2017**, 362: 36.

[6] Pontani, M., Celani, F. Neighboring optimal guidance and constrained attitude control applied to three-dimensional lunar ascent and orbit injection. *Acta Astronautica*, **2019**, 156: 78–91.

[7] Curtis, H. D. *Orbital Mechanics for Engineering Students*, 3rd edn. Butterworth-Heinemann, **2014**.

[8] Hechler, M., Cobos, J. HERSCHEL, PLANCK and GAIA orbit design. In: *Libration Point Orbits and Applications*. World Scientific, **2003**: 115–135.

[9] Colagrossi, A., Lavagna, M. Preliminary results on the dynamics of large and flexible space structures in Halo orbits. *Acta Astronautica*, **2017**, 134: 355–367.

[10] Folta, D., Beckman, M. Libration orbit mission design: Applications of numerical and dynamical methods. In: *Libration Point Orbits and Applications*. World Scientific, **2003**: 85–113.

[11] Robinson, W. J. Attitude stability of a rigid body placed at an equilibrium point in the restricted problem of three bodies. *Celestial Mechanics*, **1974**, 10(1): 17–33.

[12] Arredondo, J. A., Guo, J. G., Stoica, C., Tamayo, C. On the restricted three body problem with oblate primaries. *Astrophysics and Space Science*, **2012**, 341(2): 315–322.

[13] Zotos, E. E. Classifying orbits in the restricted three-body problem. *Nonlinear Dynamics*, **2015**, 82(3): 1233–1250.

[14] Folta, D. C., Bosanac, N., Guzzetti, D., Howell, K. C. An Earth–Moon system trajectory design reference catalog. *Acta Astronautica*, **2015**, 110: 341–353.

[15] Guzzetti, D., Howell, K. C. Natural periodic orbit-attitude behaviors for rigid bodies in three-body periodic orbits. *Acta Astronautica*, **2017**, 130: 97–113.

[16] Kane, T. R., Marsh, E. L. Attitude stability of a symmetric satellite at the equilibrium points in the restricted three-body problem. *Celestial Mechanics*, **1971**, 4(1): 78–90.

[17] Abad, A., Arribas, M., Elipe, A. On the attitude of a spacecraft near a Lagrangian point. *Astronomical Institutes of Czechoslovakia, Bulletin*, **1989**, 40(5): 302–307.

[18] Brucker, E., Gurfil, P. Analysis of gravity-gradient-perturbed rotational dynamics at the collinear Lagrange points. *The Journal of the Astronautical Sciences*, **2007**, 55(3): 271–291.

[19] Lara, M., Peláez, J., Bombardelli, C., Lucas, F. R., Sanjurjo-Rivo, M., Curreli, D., Lorenzini, E., Scheeres, D. Dynamic stabilization of L2 periodic orbits using attitude–orbit coupling effects. *Journal of Aerospace Engineering Sciences and Applications*, **2012**, 4(1): 73–81.

[20] Li, D., Liu, W., Jiang, J. The influence of orbital motion of flexible space vehicle on the dynamic traits of solar panel. In: Proceedings of the International Conference on Communications, Computing and Control Applications, **2011**: 1–5.

[21] Perdiou, A. E., Markellos, V. V., Douskos, C. N. The hill problem with oblate secondary: Numerical exploration. *Earth, Moon, and Planets*, **2005**, 97(1–2): 127–145.

[22] Peng, H., Bai, X. L., Xu, S. J. Continuation of periodic orbits in the Sun–Mercury elliptic restricted three-body problem. *Communications in Nonlinear Science and Numerical Simulation*, **2017**, 47: 1–15.

[23] Connor Howell, K. Three-dimensional, periodic, 'halo' orbits. *Celestial Mechanics*, **1984**, 32(1): 53–71.

[24] Palacián, J. F., Yanguas, P., Fernández, S., Nicotra, M. A. Searching for periodic orbits of the spatial elliptic restricted three-body problem by double averaging. *Physica D: Nonlinear Phenomena*, **2006**, 213(1): 15–24.

[25] Qian, Y. J., Yang, X. D., Zhai, G. Q., Zhang, W. Planar periodic orbits' construction around libration points with invariant manifold technique. *Proceedings of the Institution of Mechanical Engineers, Part G: Journal of Aerospace Engineering*, **2019**, 233(2): 498–509.

[26] Ceccaroni, M., Celletti, A., Pucacco, G. Birth of periodic and artificial halo orbits in the restricted three-body problem. *International Journal of Non-Linear Mechanics*, **2016**, 81: 65–74.

[27] Pontani, M., Miele, A. Periodic image trajectories in Earth–Moon space. *Journal of Optimization Theory and Applications*, **2013**, 157(3): 866–887.

[28] Giancotti, M., Pontani, M., Teofilatto, P. Earth–Moon transfers involving periodic orbits and invariant manifolds through isomorphic mapping. *Advances in the*

Astronautical Sciences, **2013**, 146: 337–352.

[29] Singh, J., Cyril-Okeme, V. U. Perturbed Robe's circular restricted three-body problem under an Oblate Primary. *New Astronomy*, **2015**, 34: 114–119.

[30] Guzzetti, D., Howell, K. C. Coupled orbit–attitude dynamics in the three-body problem: A family of orbit-attitude periodic solutions. In: Proceedings of the AIAA/AAS Astrodynamics Specialist Conference, San Diego, CA, USA, **2014**: AIAA 2014-4100.

[31] Knutson, A. J., Howell, K. Coupled orbit and attitude dynamics for spacecraft comprised of multiple bodies in Earth–Moon halo orbits. In: Proceedings of the 63rd International Astronautical Congress, Naples, Italy, **2012**: IAC-12-C1.8.1.

[32] Knutson, A. J., Guzzetti, D., Howell, K. C., Lavagna, M. Attitude responses in coupled orbit-attitude dynamical model in Earth–Moon Lyapunov orbits. *Journal of Guidance, Control, and Dynamics*, **2015**, 38(7): 1264–1273.

[33] Srivastava, V. K., Kumar, J., Mishra, P., Kushvah, B. S. Halo orbit of regularized circular restricted three-body problem with radiation pressure and oblateness. *Journal of Astrophysics and Astronomy*, **2018**, 39(5): 63.

[34] Markellos, V., Roy, A., Perdios, E., Douskos, C. N. A Hill problem with oblate primaries and effect of oblateness on Hill stability of orbits. *Astrophysics and Space Science*, **2001**, 278: 295–304.

[35] Howell, K. C. Three-dimensional, periodic, 'halo' orbits. *Celestial Mechanics*, **1984**, 32(1): 53–71.

[36] Zaborsky, S. Generating solutions for periodic orbits in the circular restricted three-body problem. *The Journal of the Astronautical Sciences*, **2020**, 67(4): 1300–1319.

[37] Guzzetti, D. Coupled orbit–attitude mission design in the circular restricted three-body problem. Ph.D. Thesis. Purdue University, **2016**.

[38] Abbasali, E., Kosari, A., Bakhtiari, M. Effects of oblateness of the primaries on natural periodic orbit–attitude behaviour of satellites in three body problem. *Advances in Space Research*, **2021**, 68(11): 4379–4397.

[39] Sabzy, S., Daneshjou, K., Bakhtiari, M. Periodic attitude motions along planar orbits in the elliptic restricted three-body problem. *Advances in Space Research*, **2021**, 67(8): 2252–2273.

[40] Brachtendorf, H. G., Melville, R., Feldmann, P., Lampe, S., Laur, R. Homotopy method for finding the steady states of oscillators. *IEEE Transactions on Computer-Aided Design of Integrated Circuits and Systems*, **2014**, 33: 867–878.

[41] Canalias, E., Masdemont, J. J. Homoclinic and heteroclinic transfer trajectories between planar Lyapunov orbits in the Sun–Earth and Earth–Moon systems. *Discrete & Continuous Dynamical Systems - A*, **2006**, 14(2): 261–279.

[42] Celletti, A., Pucacco, G., Stella, D. Lissajous and halo orbits in the restricted three-body problem. *Journal of Nonlinear Science*, **2015**, 25(2): 343–370.

[43] Tiwary, R. D., Kushvah, B. S. Computation of halo orbits in the photogravitational Sun–Earth system with oblateness. *Astrophysics and Space Science*, **2015**, 357(1): 73.

[44] Srivastava, V. K., Kumar, J., Kushvah, B. S. Regularization of circular restricted three-body problem accounting radiation pressure and oblateness. *Astrophysics and Space Science*, **2017**, 362(3): 49.

Majid Bakhtiari is an assistance professor and the head of the Multi-Satellite Space System Laboratory at the Iran University of Science and Technology. His technical researches focus on formation flying, satellite constellation design, three-body problem, distributed space systems, and space mission analysis. E-mail: bakhtiari_m@iust.ac.ir.

Ehsan Abbasali is currently a Ph.D. candidate in aerospace engineering with a minor in space engineering at the University of Tehran. He has teaching experience as a teacher assistant for three years in the areas of spacecraft's orbit–attitude motion, optimal control, and advanced optimization methods. His research specialty and interest include satellite orbit–attitude analysis, multi-body dynamics, satellite constellation, numerical computations, evolutionary optimization, and optimal control. E-mail: ehsan.abbasali@ut.ac.ir.

Siavash Sabzy received his master degree in satellite technology engineering from Iran University of Science and Technology, Tehran, Iran, in 2020. His research interest focuses on astrodynamics and celestial mechanics, including spacecraft orbit and attitude dynamics as well as periodic motions within the multi-body systems. E-mail: siavash_sabzy@alumni.iust.ir.

Amirreza Kosari received his B.S. degree from Amirkabir University, Tehran, Iran, in 1998, and his M.S. and Ph.D. degrees from the Sharif University of Technology, Tehran, Iran, in 2001 and 2008, respectively. From 2010 to 2016, he was an assistant professor with the Faculty of New Sciences and Technologies, University of Tehran, Iran. Since 2017, he is an associate professor with the same faculty. His research interests include trajectory optimization, optimal control, cooperative flights, and spacecraft attitude control. He is the author of several papers in the areas indicated above. E-mail: kosari_a@ut.ac.ir.